International Journal of Mathematics and
Computer Science, **16**(2021), no. 3, 1063–1076

Numerical Resolution of the Electrical Impedance Tomography Inverse Problem with Fixed Inclusions

Arrianne Crystal Velasco[1,2], Marion Darbas[3], Renier Mendoza[1]

[1]Institute of Mathematics
University of the Philippines Diliman
Quezon City, Philippines

[2]LAMFA CNRS UMR 7352
Université de Picardie Jules Verne
Amiens, France

[3]LAGA CNRS UMR 7539
Université Sorbonne Paris Nord
Villetaneuse, France

email: acvelasco@math.upd.edu.ph

(Received February 14, 2021, Revised June 5, 2021,
Accepted June 9, 2021)

Abstract

Electrical Impedance Tomography or EIT is an imaging technique that reconstructs the conductivity distribution in the interior of an object using electric currents. In this paper, we study the continuum model for EIT in a domain where the geometric inclusions are fixed and only the conductivity values inside these inclusions are unknown. We show analytically and numerically how the Broyden-Fletcher-Goldfarb-Shanno (BFGS) algorithm, a quasi-Newton method, can be effective in solving this inverse conductivity problem for EIT.

Key words and phrases: Electrical impedance tomography, inverse problems, quasi-newton.
AMS (MOS) Subject Classifications: 35R30, 65N30, 65K10.
ISSN 1814-0432, 2021, http://ijmcs.future-in-tech.net

1 Introduction

In Electrical Impedance Tomography (EIT), the conductivity distribution within a body is recovered based on electrical measurements around the body. Unlike x-ray tomography which exposes the subject to radiation, EIT is non-invasive and hence, a non-hazardous alternative in imaging technology. It also has the advantages of portability, low cost, and high-time resolution. EIT is a thriving area of research due to the variety of possible applications (e.g. geophysical, medical, and industrial). In particular, it is very useful in monitoring organ functions such as lungs, hearts, and brain [1, 2, 3, 4, 5].

Let Ω be a bounded simply connected domain in $\mathbb{R}^d$, $d = 2, 3$, with a smooth boundary $\partial\Omega$. In this paper, the domain Ω is considered to be a union of the background domain Ω_0 and the disjoint and fixed geometries Ω_m, $m = 1, 2, \ldots, M$, that is, $\Omega = \cup_{m=0}^{M} \Omega_i$, where $\Omega_i \cap \Omega_j = \emptyset,\ \forall\ i \neq j$.

Mathematically, EIT is divided into two parts: the forward problem and the inverse problem. In the forward problem, the electric potential u in Ω and the boundary voltage $U = u|_{\partial\Omega}$ are computed given the boundary current $f \in L^2(\partial\Omega)$ and the conductivity distribution $\sigma \in L^\infty(\Omega)$. This is done by solving the following boundary value-problem: Find u such that

$$\begin{cases} \nabla \cdot (\sigma \nabla u) = 0 & \text{in } \Omega, \\ \sigma \dfrac{\partial u}{\partial \boldsymbol{n}} = f & \text{on } \partial\Omega, \end{cases} \tag{1.1}$$

where $\boldsymbol{n}$ is the outward normal direction at $\partial\Omega$. To satisfy the conservation of charge, f is chosen so that $\displaystyle\int_{\partial\Omega} f\ dS = 0$. Moreover, the electric potential u must satisfy $\displaystyle\int_{\partial\Omega} u\ dS = 0$, which is equivalent to choosing the reference voltage. The conductivity $\sigma \in L^\infty(\Omega)$ is defined as

$$\sigma(x) = \sum_{m=0}^{M} \sigma_m \chi_m(x), \tag{1.2}$$

where $\chi_m(x)$ is the characteristic function of the subset Ω_m, and $\sigma_m \in \mathbb{R}$ with $\sigma_{\min} \leq \sigma_m \leq \sigma_{\max}$, for some positive constants $\sigma_{\min}$ and $\sigma_{\max}$. The problem (1.1) is called the continuum model for EIT [10, 12]. We focus our study on this choice. For instance, we refer the readers to [6, 10] for a presentation of other forward models for EIT.

Let us introduce the space $\tilde{L}^2(\partial\Omega) = \left\{ f \in L^2(\Omega) : \displaystyle\int_{\partial\Omega} f(\mathbf{x})\ dS = 0 \right\}$.

For a fixed boundary current $f \in \tilde{L}^2(\partial\Omega)$, we define the measurement operator $\mathcal{F} : L^\infty(\Omega) \to \tilde{L}^2(\partial\Omega)$ by

$$\mathcal{F}(\sigma) = u|_{\partial\Omega}, \tag{1.3}$$

where u is the solution of (1.1) given σ and f. Let $\sigma^\star$ be the actual conductivity distribution in Ω. The inverse problem we are concerned with, is: Given a measurement U_{obs} (observed boundary voltage), reconstruct the conductivity distribution $\sigma^\star$ such that

$$\mathcal{F}(\sigma^\star) = U_{obs}. \tag{1.4}$$

In particular, the problem consists of determining the values $(\sigma_m)_{1\leq m\leq M}$ inside the known respective inclusions $(\Omega_m)_{1\leq m\leq M}$. The background conductivity value σ_0 is assumed to be known. Though the forward problem is well-posed, the inverse problem is severely ill-posed. This is an active area of research. In the mathematical literature, the inverse problem of EIT is also known as Calderón's problem [7]. Earlier results on EIT inverse problem are focused on the identifiability question that the conductivity distribution in the domain can be uniquely determined using the entire corresponding voltage-to-current or Dirichlet-to-Neumann map. The first identifiability result for the continuum model was given by Kohn and Vogelius in [8]. Astala and Päivärinta later extended the identifiability property to an L^∞ conductivity in two dimensions [9]. For more details, we refer the readers to the review papers [10, 11].

The inverse problem is the main part of the EIT problem. In this work, we assume that the geometries Ω_m, $m = 0, \ldots, M$, defined in (1.2), are known. Furthermore, we assume that σ_0 is given (compare with [13, 17, 20]). A possible application is in monitoring the function of a body organ where the locations and geometries of the organs are already known. This can be achieved if, for example, the MRI data of the organs are available. Thus, to reconstruct σ in (1.2), we only need to determine the values of the positive scalars σ_m, $m = 1, \ldots, M$. This means that the inverse problem is reduced to determining the coefficient vector $\tilde{\sigma}$

$$\tilde{\sigma} = \{\sigma_m\}_{m=1}^M \tag{1.5}$$

such that (1.4) is satisfied. To solve (1.4), we reformulate it into a minimization problem in $\mathbb{R}^M$. We define the cost functional $J : \mathbb{R}^M \to \mathbb{R}$ as

$$J(\tilde{\sigma}) = \frac{1}{2}\int_{\partial\Omega} |\mathcal{F}(\sigma) - U_{obs}|^2 \, dS, \tag{1.6}$$

where σ depends on $\tilde{\sigma}$ because of (1.2). We propose to minimize J in (1.6) using the Broyden-Fletcher-Goldfarb-Shanno (BFGS) method, which is a gradient-based optimization algorithm. The paper is organized as follows: in the first section, we introduce the BFGS method and a convergence property. Then, we present some estimates for the solution of (1.1) and prove the local convergence of the BFGS method when applied to the minimization of J (1.6). Two− and three−dimensional numerical results illustrate the efficiency and accuracy of the proposed approach. Finally, we give some concluding remarks and perspectives for future studies.

2 The BFGS method

The BFGS algorithm belongs to quasi-Newton-type methods. Such methods use the update

$$y_{k+1} = y_k + \alpha_k d_k, \tag{2.7}$$

where $d_k = -D_k \nabla J(y_k)$ such that the matrix D_k is symmetric and positive definite. Furthermore, D_k is chosen so that the direction d_k tends to approximate the Newton direction.

Ideally, the step length α_k solves the problem $\alpha_k = \arg\min_{\alpha \geq 0} J(y_k + \alpha d_k)$. This means that a univariate minimization is done at every iteration. For computationally-expensive problems like the inverse EIT problem, this is not judicious. One alternative approach consists of using a criterion called the Wolfe's rule, that is, find α_k satisfying the two conditions

$$\begin{cases} J(y_k + \alpha_k d_k) \leq J(y_k) + c_1 \alpha_k \nabla J(y_k)^T d_k \quad \text{and} \\ J(y_k + \alpha_k d_k)^T d_k \geq c_2 \nabla J(y_k)^T d_k, \end{cases} \tag{2.8}$$

where $0 < c_1 < c_2 < 1$. The quasi-Newton method (BFGS) is summarized in Algorithm 1.

The BFGS method equipped with the Wolfe's rule for step length selection has the following convergence property.

Theorem 2.1. *Consider the iteration in* (2.7)*, where d_k is a BFGS direction vector and α_k satisfies* (2.8)*. Suppose J is bounded below in $\mathbb{R}$ and is continuously differentiable on an open set $\mathcal{N}$ containing $\mathcal{L} = \{x : J(x) \leq J(y_0)\}$ with y_0 as the initial guess. Moreover, assume that the gradient of J is Lipschitz continuous on $\mathcal{N}$, then*

$$\lim_{k \to +\infty} \|\nabla J(y_k)\| = 0.$$

Algorithm 1: BFGS QUASI-NEWTON METHOD

Input : objective function J, initial guess y_0, tolerance ϵ
Output: minimizer $y^\star$

1 Set $k = 0$, and $D_k = I_d$.

2 Set the direction vector $d_k = -\dfrac{D_k \nabla J(y_k)}{\|D_k \nabla J(y_k)\|}$, where
$D_{k+1} = D_k + \dfrac{p_k p_k^T}{p_k^T q_k} - \dfrac{D_k q_k q_k^T D_k}{\tau_k} + \tau_k \nu_k \nu_k^T$, $\nu_k = \dfrac{p_k}{p_k^T q_k} - \dfrac{D_k q_k}{\tau_k}$,
$\tau_k = q_k^T D_k q_k$, $p_k = y_{k+1} - x_k$, and $q_k = \nabla J(y_{k+1}) - \nabla J(y_k)$. Here, $\|\cdot\|$ denotes the 2-norm.

3 Find α_k that satisfies (2.8).

4 Update the estimate: $y_{k+1} = y_k + \alpha_k d_k$.

5 If $\|DJ(y_k)\| < \epsilon$ or $|J(y_{k+1}) - J(y_k)| < \epsilon$, stop. Else, $k \leftarrow k + 1$ and go back to Step 2.

The proof of the theorem above and the more detailed discussion of BFGS method can be found in [14].

3 Local Convergence Result

In this section, we present some estimates arising from the analysis of the continuum model (1.1). We also provide a brief discussion of the BFGS method. Then we show that the gradient of J is Lipschitz. We use this property to prove the local convergence of BFGS method for the minimization of J. We start with the following definition.

Definition 3.1. *Let $\sigma \in L^\infty(\Omega)$ such that $0 < \underline{\sigma} \leq \sigma(x) \leq \overline{\sigma}$, $\forall\ x \in \Omega$, for some $\underline{\sigma}, \overline{\sigma} \in \mathbb{R}$. Suppose u solves (1.1). We refer $u := u(\sigma)$ as the forward solution. Let U_{obs} be the observed boundary data. We define the adjoint solution $u^* := u^*(\sigma)$ as the solution of*

$$\begin{cases} \nabla \cdot (\sigma \nabla u^*) &= 0, & \text{in } \Omega, \\ \sigma \dfrac{\partial u^*}{\partial \boldsymbol{n}} &= \mathcal{F}(\sigma) - U_{obs}, & \text{on } \partial\Omega. \end{cases} \tag{3.9}$$

We have the following results. For the proof, we refer the readers to [12].

Lemma 3.2. *Define $\tilde{H}^1(\Omega) := \left\{ u \in H^1(\Omega) : \int_{\partial\Omega} u\ dS = 0 \right\}$ and let $f \in$*

$\tilde{L}^2(\partial\Omega)$. *The forward problem* (1.1) *has a unique solution in* $\tilde{H}^1(\Omega)$, *and the adjoint problem* (3.9) *shares this property, too. The following estimates hold*

$$\|u\|_{H^1(\Omega)} \leq C_1 \|f\|_{\tilde{L}^2(\partial\Omega)} \tag{3.10}$$

and

$$\|u^*\|_{H^1(\Omega)} \leq C_2 \left(\|f\|_{\tilde{L}^2(\partial\Omega)} + \|U_{obs}\|_{\tilde{L}^2(\partial\Omega)} \right), \tag{3.11}$$

for some positive constants C_1 *and* C_2. *Furthermore, let* $\rho, \eta \in L^\infty(\Omega)$ *be conductivity distributions such that* $0 < \underline{\sigma} \leq \rho(x), \eta(x) \leq \overline{\sigma}$, $\forall\ x \in \Omega$. *Then, we have*

$$\|\nabla u(\rho) - \nabla u(\eta)\|_{L^2(\Omega)} \leq C_3 \|\rho - \eta\|_{L^\infty(\Omega)} \tag{3.12}$$

and

$$\|\nabla u^*(\rho) - \nabla u^*(\eta)\|_{L^2(\Omega)} \leq C_4 \|\rho - \eta\|_{L^\infty(\Omega)}, \tag{3.13}$$

for some constants $C_3, C_4 > 0$.

Because BFGS method is gradient-based, we need to differentiate J. In order to do so, we need the following result. The proof can be found in [13].

Lemma 3.3. *Let* $\delta\sigma$ *be a sufficiently smooth perturbation of* $\sigma \in L^\infty(\Omega)$ *with compact support such that* $\delta\sigma|_{\partial\Omega} = 0$. *Then,*

$$\int_{\partial\Omega} \mathcal{F}'(\sigma)(\delta\sigma)(\mathcal{F}(\sigma) - U_{obs})\ dS = -\int_\Omega \delta\sigma \nabla u \cdot \nabla u^*\ dV. \tag{3.14}$$

We can now compute the gradient of J which is denoted by $DJ = \left[\dfrac{\partial J}{\partial \sigma_i}\right]_{i=1}^{M}$.

Proposition 3.4. *Let* $i \in \{1, \ldots, M\}$. *The partial derivative of* J *with respect to* σ_i *is given by*

$$\frac{\partial J}{\partial \sigma_i}(\tilde{\sigma}) = -\int_{\Omega_i} \nabla u \cdot \nabla u^*\ dV.$$

Proof. Applying chain rule on J in (1.6) and differentiating σ in (1.2) with respect to σ_i, we get

$$\frac{\partial J}{\partial \sigma_i}(\tilde{\sigma}) = \int_{\partial\Omega} \mathcal{F}'(\sigma)(\chi_i)(\mathcal{F}(\sigma) - U_{obs})\ dS.$$

We now use (3.14) by setting $\delta\sigma = \chi_i$. Clearly, χ_i has a compact support. Furthermore, $\chi_i|_{\partial\Omega} = 0$ because Ω_i is only nonzero at the boundary if $i = 0$. Thus, we have

$$\begin{aligned}\frac{\partial J}{\partial \sigma_i}(\tilde{\sigma}) &= \int_{\partial\Omega} \mathcal{F}'(\sigma)(\chi_i)(\mathcal{F}(\sigma) - U_{obs})\, dS \\ &= -\int_{\Omega} \chi_i \nabla u \cdot \nabla u^*\, dV = -\int_{\Omega_i} \nabla u \cdot \nabla u^*\, dV. \end{aligned} \tag{3.15}$$

□

To show that the BFGS method locally converges when applied to J, the following result is needed.

Theorem 3.5. *The gradient DJ of the cost functional J is Lipschitz continuous.*

Proof. Let ρ and η be conductivity distributions and denote $\tilde{\rho} = \{\rho_m\}_{m=1}^M$ and $\tilde{\eta} = \{\eta_m\}_{m=1}^M$ to be their corresponding coefficient vectors in $\mathbb{R}^M$ based on (1.2) and (1.5). It is sufficient to show that

$$\left|\frac{\partial J(\tilde{\rho})}{\partial \sigma_i} - \frac{\partial J(\tilde{\eta})}{\partial \sigma_i}\right| \leq C\|\tilde{\rho} - \tilde{\eta}\| \tag{3.16}$$

for some positive constant C and $\|\cdot\|$ the 2-norm on $\mathbb{R}^M$. Observe that by triangle inequality, the definition of the $L^\infty-$norm, and the equivalence of finite-dimensional norms, we get

$$\begin{aligned}\|\rho - \eta\|_{L^\infty(\Omega)} &\leq \sum_{m=1}^{M} \|(\rho_m - \eta_m)\chi_m\|_{L^\infty(\Omega)} \\ &= \sum_{m=1}^{M} |\rho_m - \eta_m|\, \|\chi_m\|_{L^\infty(\Omega)} = \|\tilde{\rho} - \tilde{\eta}\|_1 \\ &\leq C_5\|\tilde{\rho} - \tilde{\eta}\| \end{aligned} \tag{3.17}$$

(where $\|\cdot\|_1$ denotes the l^1-norm) for some positive constant C_5. Let us define $A := \left|\frac{\partial J(\tilde{\rho})}{\partial \sigma_i} - \frac{\partial J(\tilde{\eta})}{\partial \sigma_i}\right|$. Using Proposition 3.4, the triangle inequality,

and the fact that $\Omega_i \subset \Omega$, we get

$$\begin{aligned} A &= \left| -\int_{\Omega_i} \nabla u(\rho) \cdot \nabla u^*(\rho)\, dV + \int_{\Omega_i} \nabla u(\eta) \cdot \nabla u^*(\eta)\, dV \right| \\ &\leq \int_{\Omega_i} |\nabla u(\rho) \cdot (\nabla u^*(\rho) - \nabla u^*(\eta))| + \int_{\Omega_i} |\nabla u^*(\eta) \cdot (\nabla u(\rho) - \nabla u(\eta))|\ dV \\ &\leq \int_{\Omega} |\nabla u(\rho) \cdot (\nabla u^*(\rho) - \nabla u^*(\eta))| + \int_{\Omega} |\nabla u^*(\eta) \cdot (\nabla u(\rho) - \nabla u(\eta))|\ dV. \end{aligned} \tag{3.18}$$

We can apply the Cauchy-Schwarz inequality on the right-hand side of (3.18). The estimates (3.10), (3.11), (3.12), (3.13), and the definition of the H^1-norm give

$$\begin{aligned} A &\leq \|\nabla u\|_{L^2(\Omega)} \|\nabla u^*(\rho) - \nabla u^*(\eta)\|_{L^2(\Omega)} + \|\nabla u^*\|_{L^2(\Omega)} \|\nabla u(\rho) - \nabla u(\eta)\|_{L^2(\Omega)} \\ &\leq C \|\rho - \eta\|_{L^\infty(\Omega)} \end{aligned} \tag{3.19}$$

by combining (3.17), (3.18), and (3.19), the inequality (3.16) and by taking

$$C \coloneqq C_5 \left(C_1 C_4 \, \|f\|_{\tilde{L}^2(\partial\Omega)} + C_2 C_3 \left(\|f\|_{\tilde{L}^2(\partial\Omega)} + \|U_{obs}\|_{\tilde{L}^2(\partial\Omega)} \right) \right).$$

□

Remark 3.6. *Notice that the functional J in* (1.6) *satisfies the assumptions of Theorem 2.1 because of Proposition 3.4, Theorem 3.5, and the fact that $J \geq 0$. Hence, convergence of the algorithm to a stationary point is guaranteed. However, the convexity of the cost function J is needed to prove that the said stationary point is the one where the cost function is minimal. Unfortunately, proving that the cost function is convex is not trivial. In the next section, we show numerically that the algorithm converges to the minimizer regardless of the starting point.*

4 Numerical Implementation

We consider two−dimensional and three−dimensional numerical examples. The forward problem is solved using the Finite Element Method (FEM). Lagrange finite elements of type $\mathbb{P}_1$ are used. We implemented the numerical solver with FreeFem++ [16]. For the analysis of the numerical solution of (1.1) using FEM, we refer the readers to [19]. The inverse problem is

solved in MATLAB using the built-in command for BFGS algorithm, *fminunc*. Tolerance is set to be the default, $\epsilon = 10^{-16}$. We work with synthetic data which are obtained by solving the continnum model (1.1) with the exact conductivity distribution σ^* in Ω and an injected current f on the boundary of the object. To model possible experimental errors, a 1% additive noise is included [17]. Finally, a finite number of initial vectors y_0 (which are coefficient vectors as (1.5)) are generated in the range of the parameters. The aim is to emphasize that the algorithm for the numerical resolution of the inverse problem will still converge using different initial guesses.

Consider a two-dimensional representation of thorax using an MRI image [18]. The background conductivity is taken to be equal to $\sigma_0 = 0.67$ S.m^{-1} and the unknown parameters in this case are the conductivity values inside the lungs and the heart. We take the values $[\sigma_1, \sigma_2] = [0.1, 0.63]$S.m^{-1}, for the lungs' and heart's conductivity values, respectively, to generate the synthetic boundary data. The conductivity distribution σ and the injected current f for simulating the data are shown in Figure 1. A mesh structure with 47 579 triangular elements, 24 052 nodes was considered for the resolution of the forward problem and in order to avoid an *inverse crime*, the inverse computations are done on a different mesh with 25 297 triangular elements and 12 839 nodes. We compute the approximate solution using 2 300 different initial points inside the square $[0.5, 8] \times [1.0, 8]$. We then get their corresponding relative errors and plot them in Figure 2. We observe that the error ranges from 0.0121 to 0.0132. This shows numerically the convergence of the BFGS algorithm to the stationary point for each chosen initial couple of conductivity values. Table 1 gives the true solution, the mean approximate solution of the different approximate solutions, the mean relative error, the standard deviation of the errors, and the mean cost. The BFGS algorithm is consistent in converging to the approximate solution with minimal error and cost.

Thorax				
True solution	Mean solution	Mean error	St. dev. error	Mean cost
[1.0, 6.3]	[0.9942, 6.3835]	0.0131	2.3496E-05	0.0333

Table 1: *Thorax*. True solution, mean of the 2 300 approximate solutions, mean relative error, standard deviation of the errors, and mean cost.

We now present numerical results for the case when the domain is a unit sphere with one spherical inclusion. The background conductivity is equal to $\sigma_0 = 0.33$ S.m^{-1} and the unknown parameter is the conductivity value

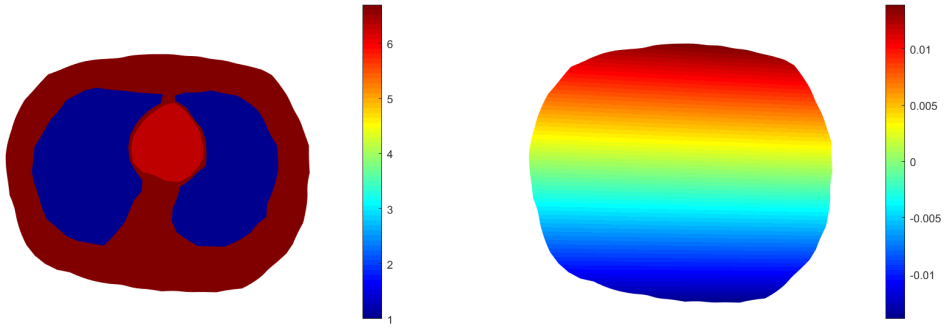

Figure 1: *Thorax.* Left: the conductivity distribution used for the generation of synthetic data. The conductivity of the lungs and the heart are respectively, σ_1 =0.1S.m^{-1} and σ_2 =0.63S.cm^{-1}. Right: the current density f injected on the boundary.

inside the perturbation. The true value is fixed to be $\sigma_1 = 1.0$ S.m^{-1}. The conductivity distribution and the injected current are given in Figure 3. The forward problem is solved using 177 032 tetrahedrons, 32 384 nodes, and 19 566 boundary triangles while the mesh for the inversion process uses 86 931 tetrahedrons, 16 356 nodes, and 11 186 boundary triangles. The approximate solution is computed using 50 different initial values in the interval from 10^{-6} to 10. We report their corresponding relative errors in Figure 4 (right). The range of the error is a small interval from 0.013076 to 0.013009. The values presented in Table 2 suggest the consistency of the algorithm.

Sphere				
True solution	Mean solution	Mean error	St. dev. error	Mean cost
1.0	1.0130	0.0130	2.6618E-07	0.1269

Table 2: *Unit sphere.* True solution, mean approximate solution of the 50 approximate solutions, mean relative error, standard deviation of the errors, and mean cost.

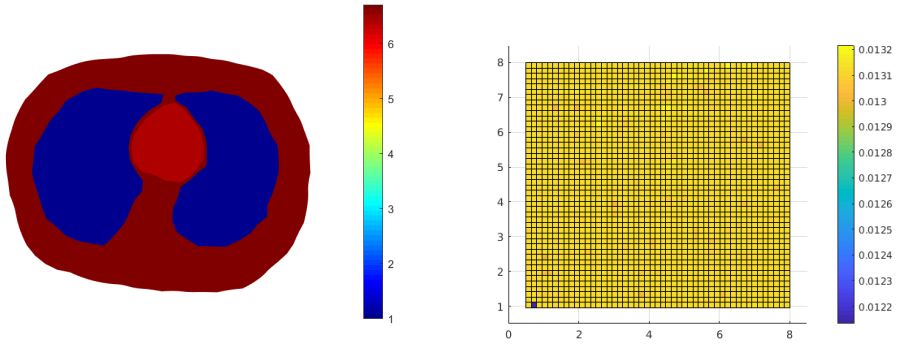

Figure 2: *Thorax.* Left: reconstructed conductivity distribution (mean of the 2 300 approximate solutions). Right: the relative errors for the 2 300 approximate solutions.

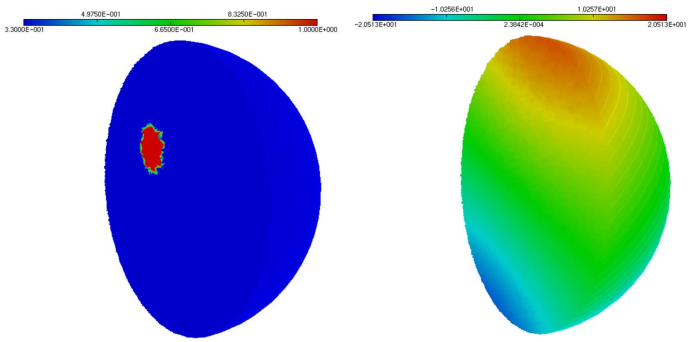

Figure 3: *Sphere.* Left: the conductivity distribution used for the generation of synthetic data. Right: the current density f injected on the boundary.

5 Conclusion and Perspectives

In this work, we studied the inverse conductivity problem in EIT where the geometry of the inclusions are known. We have shown how the BFGS method equipped with the Wolfe's rule can effectively solve such an inverse coefficient problem. We proved that the algorithm converges to a stationary point. We also showed numerically that the method converges regardless of the choice of the initial guess.

For future work, one may consider other models of the EIT, especially the Complete Electrode Model [6, 21]. Furthermore, the proof of the convexity of the cost function is still an open question.

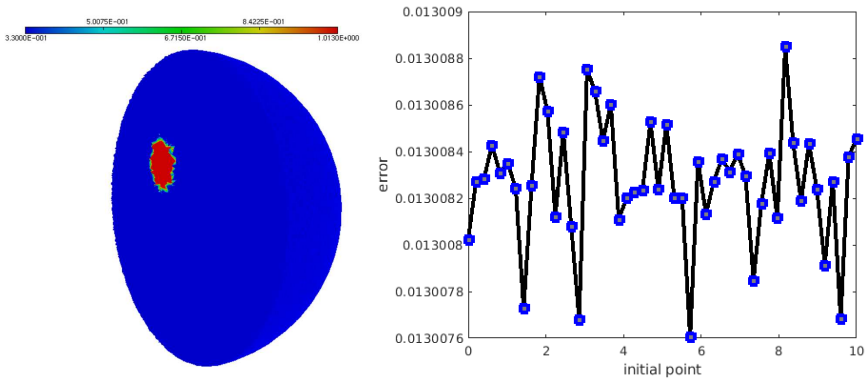

Figure 4: *Unit sphere.* Left: reconstructed conductivity distribution (mean of the 50 approximate solutions). Right: the relative errors for the 50 approximate solutions.

Acknowledgment. This work was funded by the UP System Enhanced Creative Work and Research Grant (ECWRG-2019-2-11-R).

References

[1] M. Cheney, D. Isaacson, J. Newell, Electrical Impedance Tomography, SIAM REV, **41,** (1999), 85–101.

[2] E. Teschner, M. Imhoff, S. Leonhardt, Electrical Impedance Tomography: The realisation of regional ventilation monitoring, 2nd edition, 2015.

[3] D. Holder, Clinical and physiological applications of Electrical Impedance Tomography, 1993.

[4] A. P. Bagshaw, A. D. Liston, R. H. Bayford, A. Tizzard, A. P. Gibson, A. T. Tidswell, M. K. Sparkes, H. Dehghani, C. D. Binnie, D. S. Holder, Electrical Impedance Tomography of human brain function using reconstruction algorithms based on the Finite Element Method, Neuroimage, **20,** (2003), 752–764.

[5] D. S. Holder, Electrical Impedance Tomography (EIT) of brain function, Brain Topogr., **5**, (1992), 87–93.

[6] E. Somersalo, M. Cheney, D. Isaacson, Existence and uniqueness for electrode models for electric current computed tomography, SIAM J Appl Math., **52,** no. 4, (1992), 1023–1040.

[7] A. Calderón, On an inverse boundary value problem, Seminar on Numerical Analysis and its Applications to Continuum Physics (Río de Janeiro, 1980), (1980), 65–73.

[8] R. Kohn, M. Vogelius, Determining conductivity by boundary measurements, Commun. Pure Appl. Math, **37,** (1984), 113–123.

[9] K. Astala, L. Päivärinta, Calderón's inverse conductivity problem in the plane, Ann. Math., **163,** (2006), 265–299.

[10] L. Borcea, Electrical Impedance Tomography, Inverse Problems, **19,** no. 4, (2003), 997–998.

[11] G. Uhlmann, Electrical Impedance Tomography and Calderón's problem, Inverse Problems, **25,** (2009), 123011.

[12] R. Mendoza, S. Keeling, Existence of solution for a segmentation approach to the impedance tomography problem, Electron. J. Differ. Equ., (2020), in press.

[13] R. Mendoza, S. Keeling, A two-phase segmentation approach to the impedance tomography problem, Inverse Problems, **33,** (2016), 015001.

[14] J. Nocedal, S. J. Wright, Numerical Optimization, 2006.

[15] J. F. Bonnans, J. C. Gilbert, C. Lemaréchal, C. Sagastizábal, Numerical Optimization – Theoretical and Practical Aspects, 2006.

[16] F. Hecht, New development in FreeFem++, J. Numer. Math., **20,** nos. 3-4, (2012), 251–265, https://freefem.org/.

[17] M. Hintermüller, A. Laurain, Electrical Impedance Tomography: from topology to shape, Control. Cybern., **37,** no. 4, (2008), 913–933.

[18] C. Venkatratnam, F. Nagi, Spatial resolution in Electrical Impedance Tomography: A topical review, J. Electr. Bioimpedance, **8,** (2017), 66–78.

[19] R. Mendoza, S. Keeling, FEM convergence of a segmentation approach to the electrical impedance tomography problem, AIP Conf. Proc., **1707,** no. 1, (2016), 050009.

[20] A. C. Velasco, M. Darbas, R. Mendoza, M. Bacon, J. C. de Leon, Comparative Study of Heuristic Algorithms for Electrical Impedance Tomography, Philipp. J. Sci., **149,** no. 3a, (2020), 74-7-761.

[21] M. Darbas, J. Heleine, R. Mendoza, A. C. Velasco, Sensitivity analysis of the Complete Electrode Model for Electrical Impedance Tomography, AIMS Mathematics, **6,** no. 7, (2021), 7333–7366.